Spatiotemporal Discharge Variability of the Doce River in SE Brazil During MIS 6 and 5

Iris Arndt[1]*, Silke Voigt[1], Rainer Petschick[1], Alicia Hou[2], Jacek Raddatz[1], Ana Luiza S. Albuquerque[3] and André Bahr[2]

[1]Institute of Geosciences, Goethe University Frankfurt, Frankfurt, Germany, [2]Institute of Earth Sciences, Heidelberg University, Heidelberg, Germany, [3]Departamento de Geoquímica, Universidade Federal Fluminense, Rio de Janeiro, Brazil

The modern precipitation balance in southeastern (SE) Brazil is regulated by the South American summer Monsoon and threatened by global climate change. On glacial-interglacial timescales, monsoon intensity was strongly controlled by precession-forced changes in insolation. To date, relatively little is known about the spatiotemporal distribution of tropical precipitation in SE Brazil and the resulting variability of fluvial discharge on glacial-interglacial timescales. Here, we present X-ray diffraction-derived mineralogical data for the 150–70 ka period (marine isotope stage (MIS) 6 to MIS 5) from the Doce River basin. This area was sensitive to changes in monsoonal precipitation intensity due to its proximity to the South Atlantic Convergence Zone. The data, obtained from a marine sediment core (M125-55–7) close to the Doce river mouth (20˚S), show pronounced changes in the Doce River suspension load's mineralogical composition on glacial-interglacial and precessional timescales. While the ratio of silicates to carbonates displays precession-paced changes, the mineralogical composition of the carbonate-free fraction discriminates between two assemblages which strongly vary between glacial and interglacial time scales, with precession-forced variability only visible in MIS 5. The first assemblage, dominated by high contents of kaolinite and gibbsite, indicates intensified lowland erosion of mature tropical soils. The second one, characterized by higher contents of the well-ordered illite, quartz and albite, points to intensified erosion of immature soils in the upper Doce Basin. High kaolinite contents in the silicate fraction prevailed in late MIS 6 and indicate pronounced lowland soil erosion along a steepened topographic gradient. The illite-rich mineral assemblage was more abundant in MIS 5, particularly during times of high austral summer insolation, indicating strong monsoonal rainfall and intense physical erosion in the upper catchment. When the summer monsoon weakened in times of lower insolation, the mineral assemblage was dominated by kaolinite again, indicative of lower precipitation and runoff in the upper catchment and dominant lowland erosion.
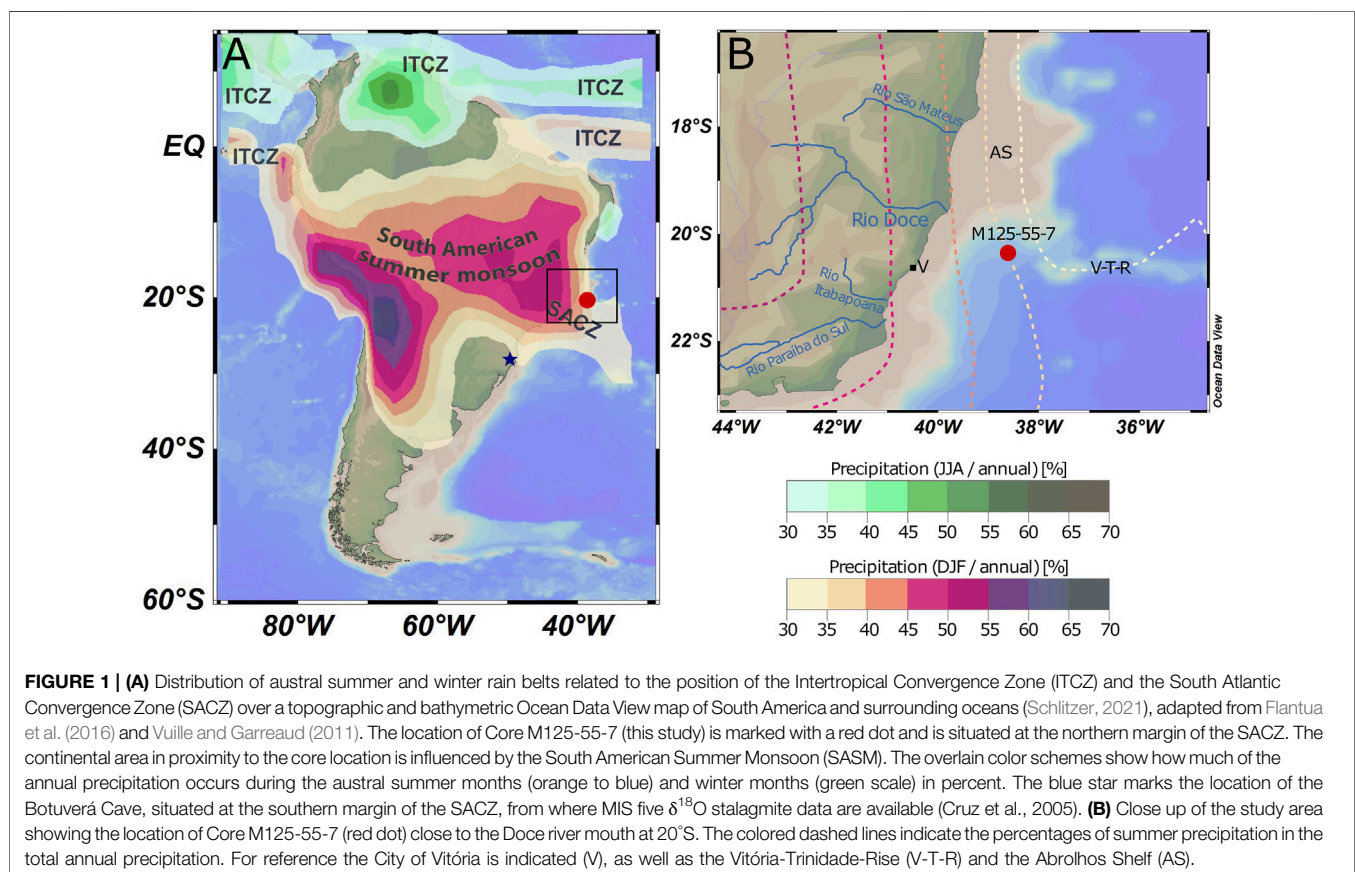
Keywords: fluvial discharge, summer monsoon, Marine Isotope Stage 6 (MIS 6), Marine Isotope Stage 5 (MIS 5), X-ray diffractometry (XRD), southeastern Brazil, western tropical Atlantic
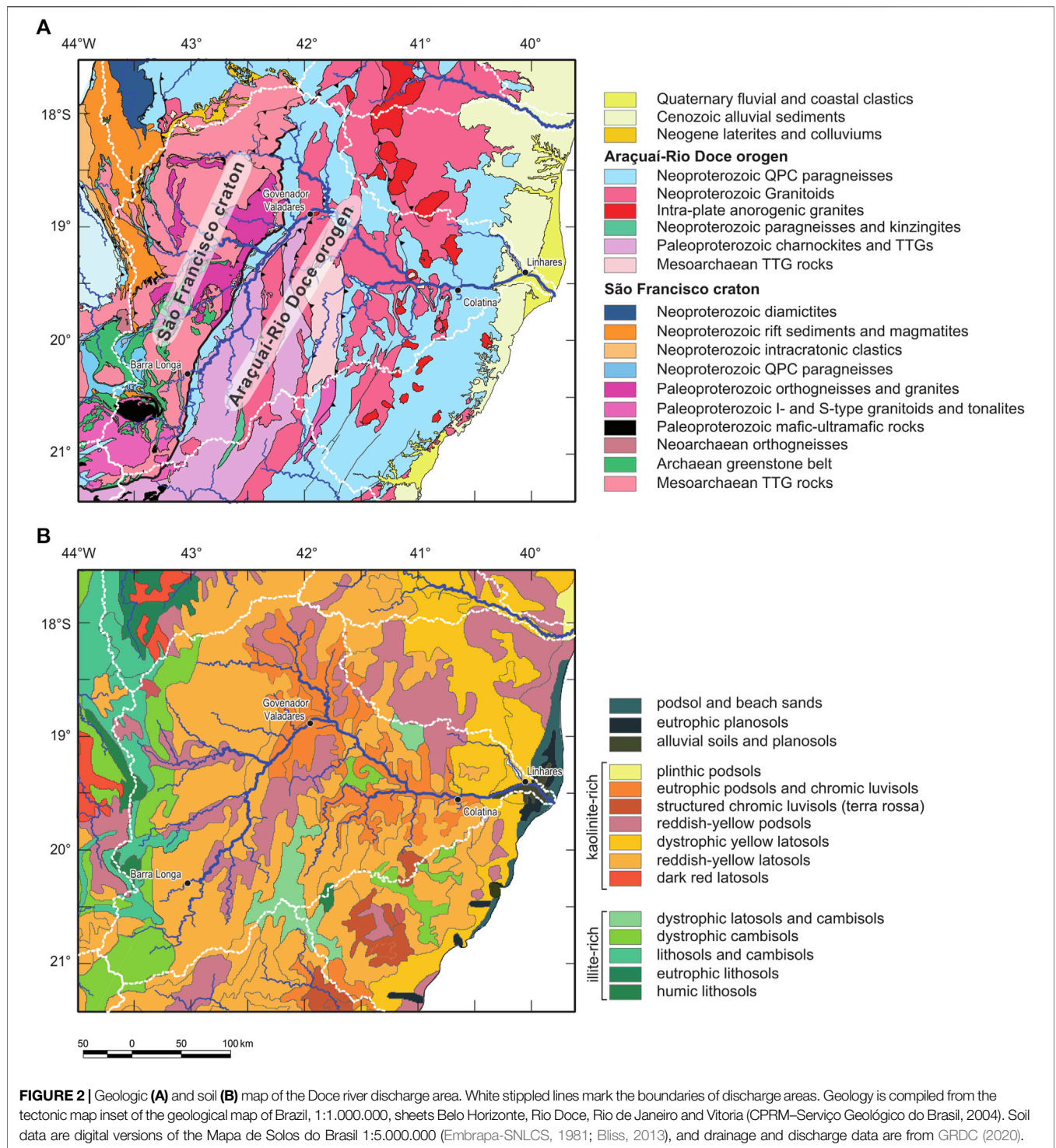
INTRODUCTION

The Doce River watershed, situated in southeastern Brazil, is considered a region strongly sensitive to climate variability and especially vulnerable to the socio-economic and environmental impacts of climate change (May et al., 2020). This region is expected to suffer from long-term droughts, flooding through heavy rainfalls, coastal erosion, which will lead to a decline in silviculture viability, reduced croplands, a loss of biodiversity, a decrease in hydroelectric generating capacity and accompanying risks to human health (May et al., 2020). Dry winters and rainy summers in the region are caused by the South American Summer Monsoon (SASM) (Carvalho, 2020; **Figure 1**). Future climate models indicate that this pattern will strengthen over eastern Brazil, leading to a further decrease in precipitation during the dry season (June, July and August) and an increase in precipitation during the rainy season (December, January and February) (FEAM, 2011; IPCC, 2021). Models for different future climate scenarios display complex, at times contradictory, spatial patterns of summer precipitation increases and decreases for the Doce Basin (FEAM, 2011). While climate model projections are constantly improving, they are still subject to uncertainties, of which some are being narrowed down and others are irreducible (Knutti & Sedláček, 2013). Uncertainties regarding regional precipitation development make regional and seasonal paleoclimate data highly valuable for estimating future precipitation patterns (Tierney et al., 2020), which is

particularly important for vulnerable regions like the Doce watershed.

Paleoclimate studies from the last glacial period and the Holocene indicate that solar irradiation and high latitude temperature changes affect South American monsoonal precipitation patterns by impacting atmospheric as well as ocean circulation and SST distribution in the tropical South Atlantic (e.g., Bahr et al., 2021; Cruz et al., 2009, 2005; Jaeschke et al., 2007; Kanner et al., 2012; Stríkis et al., 2018, 2015). In eastern Brazil, monsoon intensity over the past 300 ka was primarily controlled by precession-forced changes in insolation but also indirectly affected by changing atmospheric greenhouse gas concentrations, which can modify both the inter- and intrahemispheric temperature gradients (Rind, 1998; Hou et al., 2020a) and thereby intensity of the Hadley circulation and southeast trade winds (Seo et al., 2014). The magnitude of interhemispheric SST gradients can also play a role in determining the strength and position of the South Atlantic Convergence Zone (SACZ) (Stríkis et al., 2015), a convective band which spans from the Amazon Basin to the western South Atlantic releasing moisture provided by low level winds (Kodama, 1992). The convective activity in the SACZ and the Amazon Basin are the main components regulating the SASM (Jones & Carvalho, 2002). Therefore, changes in the strength and/or position of the SACZ impact SASM related precipitation distribution. The pattern is complicated by an additional insolation-driven east-west antiphased precipitation dipole

FIGURE 1 | (A) Distribution of austral summer and winter rain belts related to the position of the Intertropical Convergence Zone (ITCZ) and the South Atlantic Convergence Zone (SACZ) over a topographic and bathymetric Ocean Data View map of South America and surrounding oceans (Schlitzer, 2021), adapted from Flantua et al. (2016) and Vuille and Garreaud (2011). The location of Core M125-55-7 (this study) is marked with a red dot and is situated at the northern margin of the SACZ. The continental area in proximity to the core location is influenced by the South American Summer Monsoon (SASM). The overlain color schemes show how much of the annual precipitation occurs during the austral summer months (orange to blue) and winter months (green scale) in percent. The blue star marks the location of the Botuverá Cave, situated at the southern margin of the SACZ, from where MIS five δ^{18}O stalagmite data are available (Cruz et al., 2005). **(B)** Close up of the study area showing the location of Core M125-55-7 (red dot) close to the Doce river mouth at 20°S. The colored dashed lines indicate the percentages of summer precipitation in the total annual precipitation. For reference the City of Vitória is indicated (V), as well as the Vitória-Trinidade-Rise (V-T-R) and the Abrolhos Shelf (AS).

FIGURE 2 | Geologic **(A)** and soil **(B)** map of the Doce river discharge area. White stippled lines mark the boundaries of discharge areas. Geology is compiled from the tectonic map inset of the geological map of Brazil, 1:1.000.000, sheets Belo Horizonte, Rio Doce, Rio de Janeiro and Vitoria (CPRM–Serviço Geológico do Brasil, 2004). Soil data are digital versions of the Mapa de Solos do Brasil 1:5.000.000 (Embrapa-SNLCS, 1981; Bliss, 2013), and drainage and discharge data are from GRDC (2020).

occurring over tropical South America, which weakened during glacial phases (Cruz et al., 2009).

To assess the complex paleoprecipitation patterns, regional paleoclimate records are needed. Here, we provide a record of the past spatiotemporal precipitation variability in the Doce Basin, based on changes in the mineral composition of the discharged sediment analyzed via X-ray diffraction (XRD). The Doce Basin encompasses both the SACZ domain as well as the (south)eastern coastal lowlands of Brazil and thus is ideally suited to track past spatial precipitation variability. We investigated an 80 kyr time interval from late Marine Isotope Stage (MIS) 6 to the end of MIS 5, which spans over glacial, transitional and interglacial climate phases, covers a large range of CO_2 conditions (185–290 ppm V (Petit et al., 1999)) and includes several precession cycles.

CLIMATE AND GEOLOGICAL SETTING

The Doce watershed covers an area of 86,715 km². Fluvial discharge flows from elevations of over 1,500 m for roughly 850 km until reaching the Doce delta at around 19.7°S (May et al., 2020). The Caparaó mountains confine the basin to the south and the Espinhaço mountains to the west and northwest. The westernmost portion of the Doce Basin is part of the Archaean São-Francisco craton, whereas most of the basin is geologically assigned to the Proterozoic Araçuai orogen (de Almeida et al., 2000; **Figure 2**). Lithologically the basin consists predominantly of migmatites, granitoids, gneisses, schists and quartzites of Precambrian age with a few Late Proterozoic to Cambrian granitoid intrusion in the upper to middle catchment. Neogene sandstones, claystones and conglomerates cover the coastal area near the Doce river mouth (Schobbenhaus et al., 1981; **Figure 2**). In the middle to lower catchment, the rocks are overlain by thick soil layers, mainly latosols (= ferralsols, after Food and Agriculture Organization of the United Nations (FAO) classification) (**Figure 2**). In the upper mountainous regions, soils are thin and immature (FAO-UNESCO, 1971). The present-day climate in the basin is humid subtropical to tropical with dry winters and temperate to hot summers (Alvares et al., 2013), with maximum precipitation occurring in the austral summer months (December, January and February) due to the SASM. The seasonal precipitation variability leads to seasonal differences in the magnitude of water and suspended sediment discharge from the Doce River, which reach maximum values in January (Oliveira & Quaresma, 2017). Today, sediment discharge from the Doce River amounts to approximately 10 million tons per year (Lima et al., 2005; Souza & Knoppers, 2011).

While the large amounts of tropical soils in the source region make this area particularly suitable for palaeoclimate reconstructions via clay mineral analyses (Thiry, 2000), the position of the basin at the northeastern extension of the SACZ (**Figure 1**) makes its catchment sensitive to small changes in the positioning and strength of the SASM. Furthermore, the soil distribution in the Doce Basin allows for discrimination between head- and lowland-sourced sediments (**Figure 2**).

MATERIALS AND METHODS

The analyzed sediments are derived from piston gravity core M125-55–7, recovered during research cruise M125 with the German research vessel METEOR in March and April 2016. The core was taken at 20° 21.807′ S and 38° 37.387' W, 165 km from the Brazilian coast, from a water depth of 1960 m (Bahr et al., 2016). The total length of the core is 11.75 m of which a section from 2.2 to 5.2 m was sampled in steps of 2.5 cm. 119 samples with 3–9 ml of sediment material were taken from the core with open syringes. The sediment consists of greyish, greenish silty clays which are partly bioturbated and contain bioclasts. No structures within the core sediments point towards a disturbance of sedimentation by contour currents or turbidites.

Furthermore, the core location chosen is situated on a submarine hill structure identified via multibeam sounders. PARASOUND data from the uppermost 40 m of sediment show continuous parallel strata at the coring site, indicating undisturbed hemipelagic sedimentation (Hou et al., 2020a Supporting Information Figure 4S).

The age model for this core was developed by Hou et al. (2020b). The ages are based on tuning of the benthic $\delta^{18}O$ record (*Uvigerina* spp.) to the LR04 benthic $\delta^{18}O$ stack (Lisiecki & Raymo, 2005) and ^{14}C dating in the upper 120 cm (Hou et al., 2020b). Based on this age model, our data set spans from roughly 70 to 150 ka, covering the late MIS 6, termination II (T II) and MIS 5.

Sample Preparation

Approximately 2 ml (~3 g) of each sample were dried, ground by hand and filled into sample holders from the rear side to gain texture-free bulk sediment samples. The rest of each sample was dissolved in 20% formic acid and rinsed with deionized water after decarbonization. The clay-sized fraction, < 2 μm, was separated through the Atterberg method (4 cm settling height) with sodium phosphate to avoid flocculation. After retrieving the clay-sized fraction, 0.1 ml of magnesium chloride solution was added to each sample suspension. Texture-free clay samples were created by inserting the clay powder from the rear side into the sample holder. The texture-free sample XRD measurement provides data for semi-quantitative mineral phase analysis. Textured clay samples were obtained by dissolving 20 mg of the clay powder in 2 ml deionized water, pipetting the suspension on circular glass slides and letting them dry at room temperature. Data from textured samples indicate the variability in clay mineral quantity more precisely and are used for the structural analysis of illites. After being exposed to an ethylene glycol atmosphere, the textured clay samples were remeasured to expand clay minerals such as smectites. This procedure makes the illite and smectite peaks more easily distinguishable from mixed layer mineral peaks (**Figure 3**).
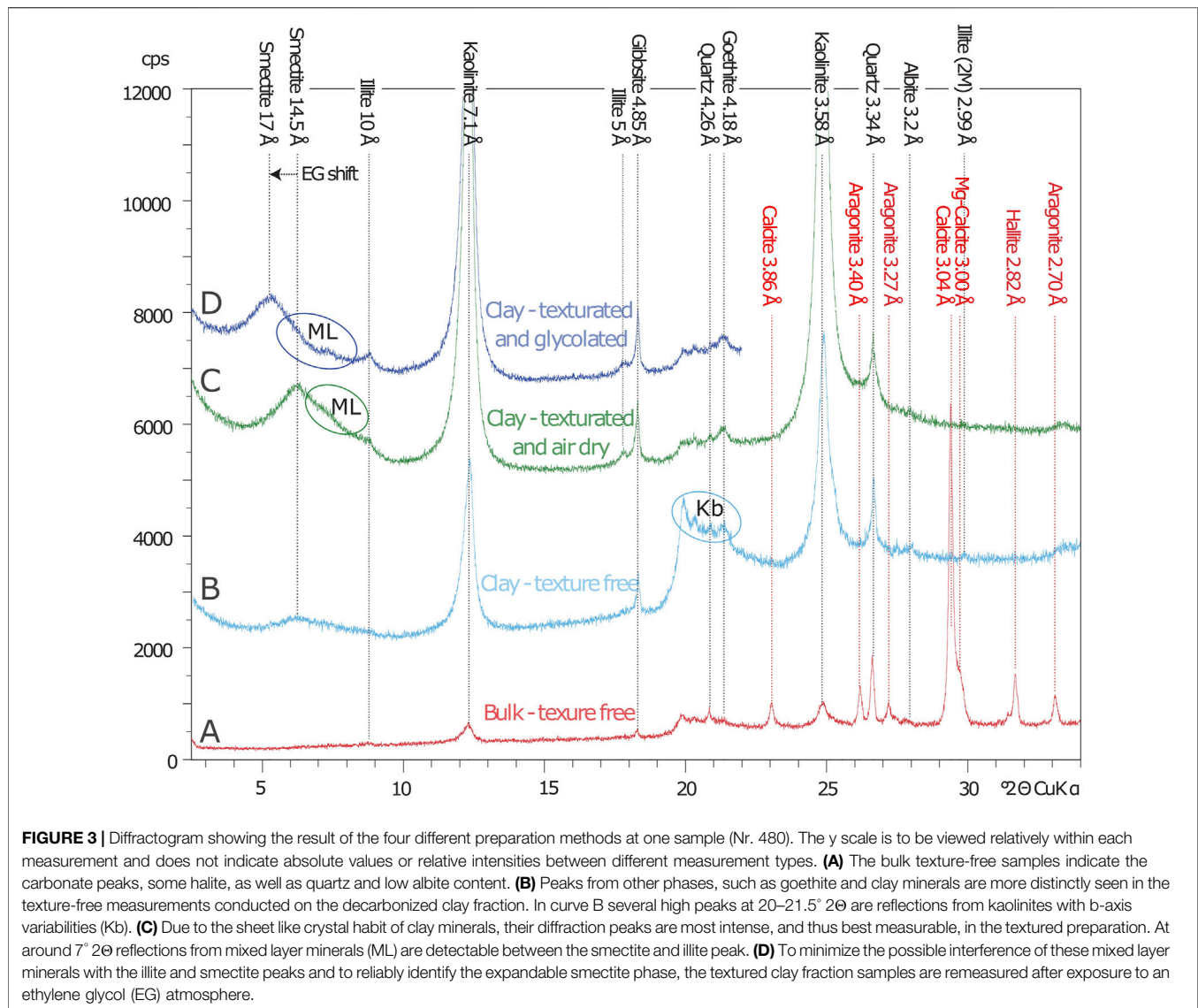
Optical Analysis

We analyzed the sieving residuals of sizes greater than 250 μm under a stereo microscope, identifying the main calcifying organisms and their superficially visible preservation state. Additionally, we prepared smear slides of the bulk sediment from equivalent core depths. The smear slides were analyzed under a Zeiss Axio Imager A2 Microscope at up to 1,250 times magnification, to evaluate the microscopic content of the samples.

X-Ray Diffractometry (XRD)

All samples were measured with a PANalytical X'Pert PRO diffractometer, equipped with a copper X-ray tube, a Ni-filter, an automatic divergence aperture, a sample spinner, a sample changer with a capacity of 15 samples and a X'Celerator detector. The measuring voltage was 40 kV and the electric current was 30 mA. Measurements were performed in steps below 0.01° 2Θ with 30–50 s per step.

Four types of XRD measurements were performed. Firstly, the whole sediment was analyzed in a texture-free manner in the bulk

FIGURE 3 | Diffractogram showing the result of the four different preparation methods at one sample (Nr. 480). The y scale is to be viewed relatively within each measurement and does not indicate absolute values or relative intensities between different measurement types. **(A)** The bulk texture-free samples indicate the carbonate peaks, some halite, as well as quartz and low albite content. **(B)** Peaks from other phases, such as goethite and clay minerals are more distinctly seen in the texture-free measurements conducted on the decarbonized clay fraction. In curve B several high peaks at 20–21.5° 2Θ are reflections from kaolinites with b-axis variabilities (Kb). **(C)** Due to the sheet like crystal habit of clay minerals, their diffraction peaks are most intense, and thus best measurable, in the textured preparation. At around 7° 2Θ reflections from mixed layer minerals (ML) are detectable between the smectite and illite peak. **(D)** To minimize the possible interference of these mixed layer minerals with the illite and smectite peaks and to reliably identify the expandable smectite phase, the textured clay fraction samples are remeasured after exposure to an ethylene glycol (EG) atmosphere.

sediment analysis. Secondly, the clay fraction only was analyzed in a texture-free manner. Thirdly, the clay fraction was analyzed with orientated particles in the textured analysis. And lastly, the textured clay samples were remeasured after exposure to an ethylene glycol atmosphere (**Figure 3**). The XRD datasets are available in the **Supplementary Material**.

XRD Data Evaluation

The XRD data is visualized in a diffractogram displaying the measured reflexes in relative counts per second (cps) over the measurement angle 2Θ for each sample (see **Figure 3**). The changes in abundance of a mineral phase were evaluated by measuring the peak intensity (texture-free samples) or the peak area (textured samples). The software used for data evaluation is MacDiff 4.2.6 (Petschick, 2010). Peak intensity measurements were applied to gain semi-quantitative sediment composition data from the texture-free samples. For the necessary peak intensity correction, we used Reference Intensity Ratios (RIRs)

from Powder Diffraction File™ 4 (PDF-4). Peak area measurements were applied to determine the relative abundance of clay mineral phases within the textured samples. For the peak area correction, Biscaye factors were used (Biscaye, 1965).

The values of the peak heights or areas of all measured phases were summed for each sample and defined as 100% of the sediment (e.g., for the bulk sediment in **Figure 4I**). The relative percentages of the phases are calculated thereafter. Aragonite, Mg-calcite and calcite are additionally evaluated separately as percentages of the sum of all carbonate phases from the bulk sediment.

RESULTS

The carbonate to silicate ratio indicates an insolation-paced relative increase in terrestrial material within the sediment
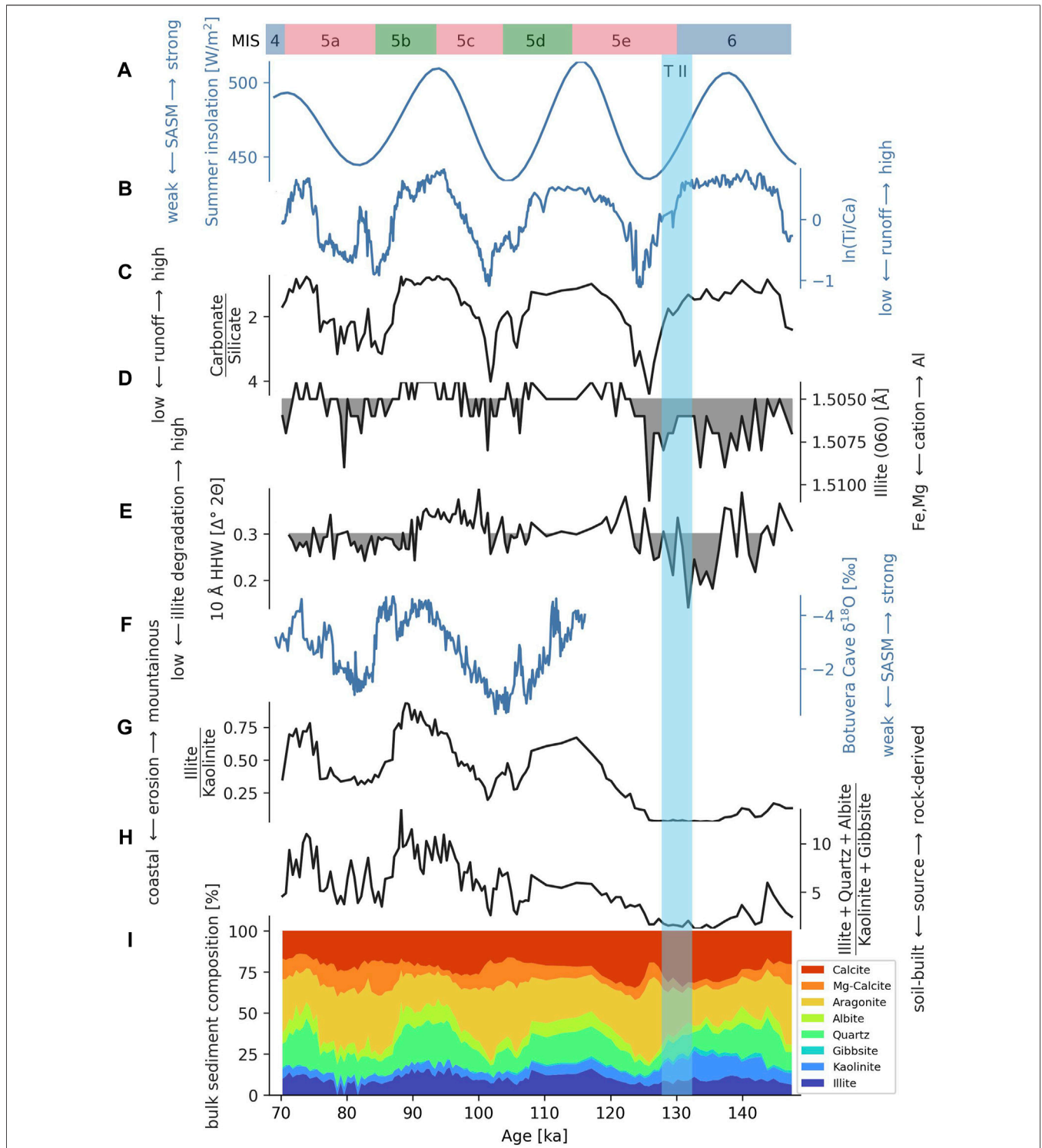
FIGURE 4 | Bulk sediment and river derived fraction XRD data compared to **(A)** the summer insolation curve at 20°S (Laskar et al., 2004), **(B)** ln (Ti/Ca) ratios based on x-ray fluorescence scanning of Core M125-55-7 (Hou et al., 2020a). **(C)** The carbonate to silicate ratio is calculated from the bulk sediment measurements and indicates the relative discharge of terrestrial material through runoff. During high insolation phases, discharge is enhanced. **(D)** The (060) peak around 1.50 Å (texture free clay fraction) indicates the proportion of different elements occupying the octahedra cation position in illite, with Fe^{2+} and Mg^{2+} indicating wider spacing and Al^{3+} lower spacing. Values above 1.505 Å are shaded. Al-rich illites are more abundant in phases of high discharge in MIS 5. **(E)** The width of the 10 Å illite peak at half of its maximum height is expressed as the half height width (HHW) within the textured clay fractions. Values below 0.3 Δ° 2Θ are shaded. Brought 10 Å peaks indicate higher degradation or lower crystallinity, occurring predominantly in high insolation phases. **(F)** δ¹⁸O values from the Botuverá Cave (cave location see **Figure 1**) from Cruz et al.

(Continued)

FIGURE 4 | (2005). **(G)** The Illite to kaolinite ratio is calculated from the textured clay fraction measurements. It represents the discharge proportion from the mountainous region, with immature, illite rich soils to the mature kaolinite rich soils of the lowlands and coastal areas where soils are particularly low in illite. Erosion in mountainous areas seems to be enhanced during interglacial high insolation phases. **(H)** Quartz, albite and illite are mainly derived from disintegrated parent rock grains within immature soils while kaolinite and gibbsite are newly built in mature soils. Their ratio is calculated from texture-free clay fraction measurements and indicates the proportion of parent rock to soil sourced discharge. **(I)** Proportion of all mineral phases determined from the bulk sediment measurements.
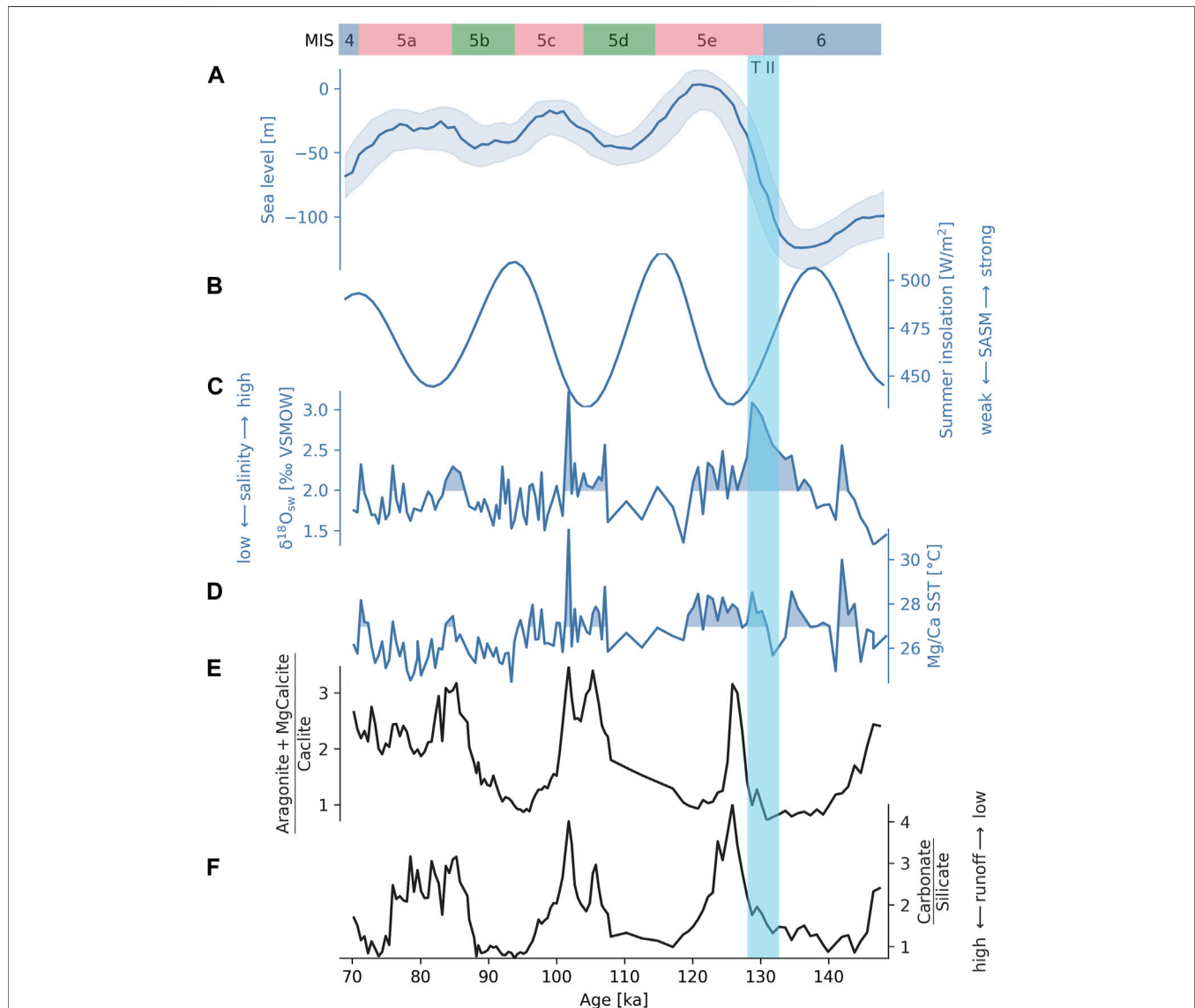
FIGURE 5 | Proportion of calcite phases compared to environmental proxies. **(A)** Sea level curve relative to today from Spratt and Lisiecki (2016). **(B)** Austral summer insolation curve at 20°S (Laskar et al., 2004). **(C)** Ice-volume-free seawater $\delta^{18}O$ curve from Core M125-55–7 (Hou et al., 2020a). **(D)** *Globigerinoides ruber* (pink) Mg/Ca SST from Core M125-55–7 (Hou et al., 2020b). **(E)** Relation of the carbonate phases aragonite and Mg-calcite to calcite. The ratio is intensifying the carbonate trends seen in the bulk sediment record (**Figure 4I**), with aragonite and Mg-calcite being decreased and calcite being increased in high insolation phases. **(F)** The carbonate to silicate ratio indicates the discharge intensity of the Doce River. The remarkable co-variability of carbonate phase proportions and discharge indicates that the riverine influx impacts the marine environmental conditions. High discharge seemed to be more profitable for calcitic organisms while in times of higher evaporation, indicated by high temperatures and salinities, aragonitic and Mg-calcitic organisms dominate the carbonate production.

(**Figures 4A–C**). The ratio of illite, quartz and albite to kaolinite and gibbsite within the bulk sediment was low during MIS six but increased during MIS 5 (**Figure 4H**). During MIS 6, illite to kaolinite is very low, while MIS 5 has a higher background illite to

kaolinite ratio (**Figure 4G**). During MIS 5, the illite to kaolinite ratio increases and decreases in phase with insolation. Similarly, the mineral phases illite, quartz and albite are dominant in the bulk sediment during MIS 5 in times of high insolation, while

kaolinite and gibbsite are relatively reduced. Furthermore, the illite to kaolinite ratio displays an asymmetric pattern with a gradual increase followed by a rather abrupt decline, as seen at 108 ka and 87 ka. A similar pattern is visible in the illite, albite and quartz to kaolinite and gibbsite ratio.

Further investigations on the half height width of the 10 Å illite peak of the textured clay fraction indicated that all illites are relatively well crystallized, with half height widths of below 0.4 Δ° 2Θ (**Figure 4E**). Using the illite polytype quantification approach after Grathoff and Moore (1996) on the texture-free clay samples, indicates that most illites (>90%) are of the 2M type, indicating growth as micas under high temperatures, whereas roughly 8% are 1M illites, typically formed in soils. The 5 Å to 10 Å illite ratios fluctuate around a value of 0.5, pointing to illites with mainly Al^{3+} as octahedral cation. Values greater than 0.4 indicate aluminum-rich illites while decreasing values signify an increasing magnesium and iron content (Esquevin, 1969). Similarly, the position of the (060) illite peak indicates the dominance of aluminum-rich illites, especially during high discharge phases (**Figure 4D**).

Aragonite, present at 35–63%, is the most abundant within the carbonate phases. Aragonite suppliers present in the samples are pteropod shells and a few other gastropod and bivalve shells. The shells are well preserved and did not show superficially visible signs of dissolution. Mg-calcite, mainly supplied by echinoderms and some miliolid foraminifera, makes up 5–28% of the carbonates. Calcite is delivered by benthic and planktonic foraminifera as well as coccolithophores and accounts for 22–58% of the carbonate fraction. In times of lower insolation, aragonite and Mg-calcite are the dominant carbonate phases, while in times of higher insolation, aragonite and Mg-calcite contents decrease, and calcite is relatively more abundant. This variability is well observed in the aragonite plus Mg-calcite to calcite ratio (**Figure 5E**). The sharp peak at 126 ka is especially rich in aragonite and is followed by a peak in calcite at around 123 ka (**Figure 4I**). This pattern is repeated less intensely during later intervals of carbonate phase development, wherein aragonite and Mg-calcite peaks at 106 and 88 ka are followed by calcite increases at 100 and 82 ka, respectively.

DISCUSSION

Mineral Phase Origins

To determine the relationship between mineralogical changes in the sediments and precipitation changes in the hinterland, it is necessary to evaluate the main origins of the mineral phases. Possible mineral sources can be categorized into terrestrial sources and marine sources. Marine sources are mainly skeletal remains of marine organisms. Terrestrial sources are more diverse; they include terrestrial material delivered from distal sources via marine currents and material from the Doce watershed and adjacent regions. The majority of the Doce watershed area is covered by thick mature soils, mainly latosols and podzols (**Figure 2**). In these mature soils, weatherable parent rock minerals are dissolved, and kaolinite and gibbsite are built (WRB, 2015). The formation of illites within

the soil could be a result of orthoclase weathering (Meunier and Velde, 2004). In the mountainous regions of the upper catchment, soils are less mature (FAO-UNESCO, 1971). Due to the less intense petrogenesis the present lithosols and cambisols contain a higher percentage of parent rock fragments. A large percentage of the Doce watersheds lithology are felsic rocks like granitoids and gneisses (**Figure 2**). Therefore, we consider muscovite, quartz and albite as likely parent rock fragments. Below we will discuss the main origins of the mineral phases measured in our samples and categorize them into four groups of origin: 1. marine built: aragonite, Mg-calcite and calcite; 2. distal sources: smectite and chlorite; 3. immature soil derived material: illite, albite and quartz; 4. mature soil derived material: kaolinite and gibbsite.

1. Marine built: The measured carbonate phases in the samples are aragonite, Mg-calcite and calcite. Noticeable terrestrial input is unlikely, as there are no significant amounts of limestone outcropping in the Doce watershed (Schobbenhaus et al., 1981). Moreover, the amount of visible clastic, non-biogenous carbonate grains in the samples was below 1%. The main mature soils present (ferralsol and acrisol) are acidic (WRB, 2015; FAO-UNESCO, 1971), prohibiting intense soil carbonate formation. Typical regional soils have low pH values of four–six and are often limed to make them suitable for agriculture (Abreu Jr et al., 2003; Santos et al., 2014). Thus, soil carbonates are not considered a significant contributor to carbonate preserved in the marine sediments. Bacterial carbonate precipitation is possible (e.g., Kranz et al., 2010) but scarce in Cenozoic open marine environments (Riding, 2000). We do not expect it to be a substantial carbonate contributor but cannot exclude a contribution to the micritic carbonate ooze. We analyzed the bulk sediment samples microscopically, and they consisted of both planktic (coccolithophores, foraminifera, gastropods) and benthic (foraminifera, echinoderms, gastropods, bivalves) calcifying organisms. Overall, the carbonate phases contained in the sediment seem to be mainly built by calcifying organisms.

2. Distal sources: Smectite and chlorite are detectable in the clay samples. They are, however, not present in the clay fraction transported by the Doce River (Tintelnot, 1995) nor are they typically built in tropical soils, but rather indicative for dryer and cooler climates (Velde, 1995). They likely originated from soils in south Brazil and Argentina (smectite) and the Patagonian region (chlorite) from where they were transported northward to the core site via marine currents (Jones, 1984; Petschick et al., 1996; Warratz et al., 2017). As they are not discharged from the Doce Basin and thus not indicative of regional climate variability, they are not further discussed.

3. Immature soil derived: Illite polytype quantification after Grathoff and Moore (1996) indicates that over 90% of the illites in the analyzed sediments originate from ground muscovite (M2 type), while only 8% are newly formed in soils (M1 type). The illite crystallinity, measured via the half-height widths of the 10 Å illite peak, provides another indicator for their origin. Low half height widths, below 0.4 Δ° 2Θ, point towards an illite development from fine-grained mica (Velde & Meunier, 2008). All samples have illite crystallinity values below 0.4 Δ° 2Θ and even decrease below 0.2 Δ° 2Θ during late MIS 6. High 5 Å to 10 Å illite peak ratios, around 0.5, indicate aluminum-rich illites

(Esquevin, 1969), also pointing towards a muscovite origin. The mineralogical illite parameters suggest the parent rocks provided for most of the illite contained in the sediment, while soil-built illites were a minor contributor. Most mature soils in the Doce watershed contain only approximately 3% mica. The soils on the coastal, Neogene clastic sediments have even lower mica concentrations of around 0.1% (Melo et al., 2001). However, the percentage of illite relative to all clay minerals transported in the Doce River is approximately 20% (Tintelnot, 1995). The discrepancy between the illite content of the mature soil and the detrital river discharge underlines that another significant source of illite must be present, in this case, the thin and immature soils of the upper catchment. Quartz and albite, like illite, originate from weathered parent rock and are present in regional soils. Higher quartz and albite concentrations are however expected in the immature soils of the upper catchment, due to lower rates of chemical weathering. Weatherable minerals, like feldspars, are usually scarce or absent in the mature ferralsols, while quartz can sustain this intense weathering (WRB, 2015). The covarying behavior of quartz, illite and albite indicates that these phases are delivered *via* a similar process. It is expected that through enhanced erosivity during heavy precipitation events, more parent rock derived mineral phases from the immature soils of the mountainous hinterland are transported to the ocean. Overall, we assume that the major proportion of the parent rock derived grains (illite, quartz, and albite) are delivered from erosion in mountainous areas with shallow soils while only a small proportion comes from the mature soils in the lowlands, making these mineral phases indicative of input from immature soils.

4. Mature soil derived: Kaolinite is newly built during ferralsol formation (WRB, 2015), and ferralsols/latosols are the most abundant mature soils in the Doce Basin (FAO-UNESCO, 1971; **Figure 2**). Gibbsite is typically formed under high weathering regimes and is also a common phase in ferralsols (Mohr et al., 1972; Sanchez, 2019). The regional mature soils have kaolinite contents of 50–80% (Melfi et al., 1983; Cunha et al., 2019), while in the sediment load of the Doce River, close to the river mouth, kaolinites make up approximately 80% of the transported clay minerals (Tintelnot, 1995). Kaolinite and gibbsite are thus indicative of material derived from regional mature lowland soils.

On the eastern and southeastern Brazilian coast, the Doce River is associated with the highest suspended sediment discharge into the Atlantic Ocean (Lima et al., 2005; Souza & Knoppers, 2011) and is the river mouth closest to the core site. Additionally, the ratio of illite to kaolinite at the coring depth of ~2,000 m, matches that of the shelf and the Doce River itself. The smaller São Mateus River, adjacent to the north (**Figure 1**), shares a similar illite to kaolinite ratio (Tintelnot, 1995). The nearest river with a similarly large catchment area and sediment discharge to the Doce River is the Jequitinhonha River mouthing into the South Atlantic at around 16°S (Souza and Knoppers, 2011). This river has an illite to kaolinite signature twice as high and the illite to kaolinite ratio of the even larger São Francisco River, mouthing at ~ 10°S, is over four times higher than that of the Doce River

(Tintelnot, 1995). At present, it appears that the Doce River is the main regional supplier of terrestrial sediment deposited at the continental slope at 20°S. The satellite analysis of regional riverine turbidity plumes underlines this assumption, as the suspended material of smaller rivers to the north of the Doce River is contained on the inner shelf while the Doce River delivers material to the offshore region (Oliveira et al., 2012). In times of low sea levels, however, more input from the coastal areas adjacent to the Doce watershed can be expected. A deposition of small amounts of sediment from smaller catchments with similar mineral compositions transported by the southward flowing Brazil Current cannot be ruled out. However, adjacent catchments are significantly smaller and supply less sediment. Therefore, we argue that the Doce catchment is the main supplier of regional terrestrial sediment to the coring site and changes in the terrestrial mineral assemblage of the core sediment are caused by changes in the Doce River discharge composition.

Within the Doce watershed, a regional distribution of different mineral sources allows for the discrimination between three areas: the mountainous regions with thin immature soils in the upper catchment as the source for most of the illite, quartz and albite; the mature, thick soil plains of the middle and lower catchment, being low in illite and rich in kaolinite; and the almost illite-free coastal lowland soils (Melo et al., 2001) supplying mainly kaolinite. A distinction between the two endmembers (i.e., mountainous vs. coastal erosion) can be seen in the illite to kaolinite ratio (**Figure 4G**).

Carbonate Variability

Within the carbonate phases, a distinct insolation-related pattern is visible (**Figure 5**). Aragonite and Mg-calcite proportions are higher in times of low summer insolation and low fluvial discharge. In contrast, calcite is increased in times of high summer insolation and higher fluvial discharge. The rise of aragonite and Mg-calcite productivity in MIS five corresponds to some degree with elevated SST and salinity ($\delta^{18}O$ ice-free seawater) data from the same core (Hou et al., 2020a; **Figures 5C–E**).

At the core site, the lowest water mass is the Upper North Atlantic Deep Water (UNADW), which is present from the ocean floor (1,960 m) to depths of roughly 1,100 m (Bahr et al., 2016). The lower boarder of the UNADW lies around 2,500 m in this region (Henrich et al., 2003). Antarctic Intermediate Water (AAIW) flows at depths of 600–1,100 m (Bahr et al., 2016). Carbonate deposition at the core location occurred at a depth of ca. 2,000 m, which is well above both the tropical West Atlantic aragonite compensation depth (3,400 m) and the lower aragonite lysocline (2,500 m) (Gerhardt & Henrich, 2001). It has been reported that due to high fluvial nutrient input at around 19 to 23°S, primary productivity is elevated and metabolic CO_2, formed by respiration of the organic matter, can acidify the already slightly carbonate undersaturated AAIW. Therefore, aragonite dissolution can occur at above 1,330 m water depth in that area (Gerhardt & Henrich, 2001). Presently, aragonite is well preserved at water depths around 2,000 m in the western South Atlantic. During the last glacial maximum, preservation at this depth was very good to moderate (Henrich et al., 2003). The

shells we recovered through sieving appeared macroscopically well preserved and further dissolution analysis was not performed. At roughly 30°S, Petró et al. (2021) analyzed supra-lysoclinal carbonate dissolution from MIS 5 to MIS 1, by analyzing foraminifera fragmentation. They report good preservation at roughly 1,500–2,000 m water depths for MIS 5. Furthermore, (aragonitic) scleractinian cold water corals are presently growing at around 900 m water depth. These corals even profited from strong runoff and higher nutrient availability during glacial periods (Bahr et al., 2020; Raddatz et al., 2020). We therefore assume a low aragonite solubility at the deposition site during both glacial and interglacial periods as well as low dissolution in the water column. Although, it cannot be excluded that some aragonite dissolution took place as aragonitic shells sank through the carbonate under-saturated AAIW, we argue that dissolution is not the driver for changes in the carbonate composition nor the carbonate to silicate ratio.

Since aragonite dissolution at the deposition site was probably low to moderate, the aragonite and Mg-calcite to calcite ratio likely reflects the relative productivity changes of the different calcifiers. Aragonite and Mg-calcite calcifiers could have been better adapted to elevated temperatures and salinities and less tolerant to increased nutrient levels and turbidity induced by high fluvial discharge. By contrast, calcitic organisms could have thrived in times of high summer insolation and higher fluvial discharge. The calcareous nannofossil assemblage from a nearby core (KF-12, taken at ~21°S) consists of over 60% opportunistic coccolithophores (*Emiliania huxlei* and *Gephyrocapsa* spp.) (Costa et al., 2016). In times of high fluvial discharge, Costa et al. (2016) saw an increase in these species, indicating higher surface water productivity due to a shallowing nutricline. The relatively high calcite proportion seen in our samples during enhanced fluvial discharge phases could similarly be caused by an increase in opportunistic coccolithophore species due to their ability to adapt better to nutrient enrichment in the surface water.

Monsoon Driven Discharge Variability During MIS 5

The carbonate to silicate ratio can be driven by carbonate productivity, carbonate dissolution, and terrestrial input variability. In times of high fluvial nutrient influx, an increase in primary productivity and respiration is expected, which could lead to acidification of the water masses and carbonate dissolution (Jahnke et al., 1994; Suárez-Ibarra et al., 2022). Runoff-dependent aragonite dissolution would drive the carbonate to silicate ratio in the same direction as increased fluvial sediment influx. Thus, carbonate dissolution, if present, enhances the relative silicate content. Runoff enhanced primary productivity could also increase the overall carbonate production and sedimentation rates. As such the impact of carbonate productivity could have a major impact on the carbonate to silicate ratio. Costa et al. (2016), however, observed a negative correlation between calcareous nannofossil productivity and the carbonate content in the fine fraction in their data, indicating dilution by terrestrial input in times of increased runoff. The core from Costa et al. (2016) was collected from less than 200 km south of M125-55-7

and includes sediments from 50 to 140 ka. Their core position is further from the Doce river mouth and closer to the mouth of the Paraiba do Sul, a river that nowadays has less than half of the Doce River's yearly fluvial discharge (Lima et al., 2005). We assume that our core's sediments are similarly or even more strongly controlled by fluvial sediment influx than the core studied by Costa et al. (2016). Therefore, we argue that the carbonate to silicate ratio can be used to indicate the fluvial discharge intensity of the Doce River.

The carbonate to silicate ratio indicates an increased overall fluvial discharge during intervals of high austral summer insolation and confirms the previously measured ln (Ti/Ca) (Hou et al., 2020a). Its insolation dependence appears to be more robust during MIS 5 (**Figure 4**). A strengthening of the monsoon system during high insolation periods of the MIS 5 interglacial would have caused heavy seasonal precipitation in the Doce watershed. Intense summer monsoon precipitation may have increased the erosivity of the Doce River, especially in the Espinaço and Caparaó mountains in the western and southern upper and middle catchment. Increased transport of disintegrated parent rock material from immature soils would be expected in this scenario and is confirmed by the mineral composition of the discharge in high insolation phases of MIS 5. While carbonate to silicate ratios decrease, the immature soil derived phases albite, quartz and illite are relatively increased (**Figure 4H**). The high illite to kaolinite ratio and illite mineral parameter development during high insolation intervals (**Figures 4D,G**) underline the notion that erosion in the mountainous hinterland is enhanced in MIS 5 high insolation periods.

The illite crystallinity, indicated by the half-height width of the 10 Å illite peak, refers to the amount of consecutively stacked illite crystal layers. Illite crystallinity is generally high in Core M125-55-7 sediments, indicating that illites are mostly crushed mica particles (Velde & Meunier, 2008). Still, a slight decrease can be seen during high insolation phases of MIS 5. A reduced crystallinity could indicate an increased supply of soil-built illites in times of high insolation or stronger weathering of the parent rock in immature soils, delivering more degraded illites. Illite polytype quantification indicates that only a low proportion of illites (8%) could be soil-built (1M type). Therefore, we assume that a decrease in crystallinity mainly indicates increased muscovite comminution due to intensified weathering in mountainous regions. High insolation phases in MIS 5 co-occur with an increase in aluminum at the octahedral cation position, as indicated by a lower illite (060) peak position (**Figure 4D**). This could be a sign of stronger illite degradation, promoting a reduction of Fe in illite through leaching in times of high insolation and increased monsoonal precipitation. High illite degradation, the increased proportion of aluminum-rich illites and the overall increase in illites in the discharged sediment indicate increased erosion from mountainous regions, suggesting an increase in heavy precipitation events in these regions. It is thus likely that a strong summer monsoon, similar to the present-day SASM, developed during the high insolation phases of MIS 5. As insolation maxima were higher during MIS 5 than they are

nowadays in MIS 1 (Laskar et al., 2004), the summer monsoon during MIS 5 was likely more intense than the present-day SASM.

During the low austral summer insolation phases of MIS 5, discharge from the Doce River decreased as indicated by the carbonate to silicate ratio increase. High illite crystallinity also points to lower illite degradation in low insolation phases. Furthermore, there was a reduction in the proportion of parent rock derived fraction to soil-built fraction. A decrease in erosivity and weathering indicates reduced water availability, which we interpret as a weakening of the summer monsoon system during the low insolation phases of MIS 5. The low illite to kaolinite ratio supports our interpretation that, due to a weakened summer monsoon, erosion in the upper river course is reduced, making mature lowland soils the primary supplier for the fluvial sediment load. At the same time, SE trade winds and with them austral winter precipitation could have increased in MIS 5 low insolation phases similar to the situation in MIS 6 proposed by Hou et al. (2020b). An intensification in coastal precipitation would further support the erosion of illite depleted, kaolinite rich coastal soils.

The asymmetry of the illite to kaolinite curve indicates a slow increase in mountainous erosion, driven by a gradually intensifying monsoon, followed by a rapid decrease in the ratio of illite to kaolinite as monsoonal precipitation weakened. A similar pattern is visible in the ratio of parent rock derived minerals to soil-built minerals (**Figure 3H**). It is to be noted that a continuation of the heavy monsoon signal during already decreasing insolation takes place at the beginning of the cooler substages MIS 5d and MIS 5b. This could be an indicator of higher moisture availability in the Doce Basin during global cooling. The overall tendency of the system for a slow moisture increase followed by a rapid decrease in moisture availability, as shown in our data, highlights the region's potential vulnerability to increasing droughts in a changing climate (May et al., 2020).

To assess the spatial variability in monsoonal rainfall intensity, we compared our data to a $\delta^{18}O$ stalagmite record from the Botuverá Cave (Cruz et al., 2005), which is located around 28°S, near the coast of southern Brazil and at the south margin of the SACZ (see **Figure 1**). The effect of the insolation driven strength of monsoonal precipitation on the $\delta^{18}O$ values from the Botuverá Cave and the illite to kaolinite ratio from the Doce watershed are in phase (**Figures 4F,G**). As these two sites are located on the opposite margins of the SACZ, we assume that the monsoonal system weakened and strengthened with insolation variability during MIS five rather than being displaced latitudinal.

Lowland Discharge During Late MIS 6

Like during MIS 5, an increase in sediment discharge during phases of high summer insolation is visible during MIS 6. However, the dominance of parent rock derived material from immature soils over mature soil-built mineral phases during the high insolation period is missing. Also, the illite to kaolinite ratios, which showed a clear covariation with insolation in MIS 5, stay continuously low throughout MIS 6 and are well below the values from low insolation phases during MIS 5. This could be an indicator of stronger erosion in the illite-depleted present-day coastal areas and the widely exposed Brazilian shelf area during MIS 6 (Maia et al., 2010; Bastos et al., 2016), due to sea levels of more than 100 m below present (Spratt & Lisiecki, 2016). At low sea levels the Doce

catchment would expand to include more of the present coastal and shelf areas. During the period of reduced illite input in MIS 6, illites show more variable but overall higher iron and/or magnesium contents and higher crystallinities (**Figures 4D,E**). This indicates that the delivered illites derive mainly from crushed muscovite in lower soil layers close to the parent rock. A steeper topographic gradient at an exposed shelf could have induced erosion of low soil layers at times exhibiting some better-preserved parent rock derived material, like illites with higher crystallinities. The increased variability underlines a more diverse, lower soil origin of the few illites eroded during MIS 6, in contrast to the more stable and abundant supply of illites from the immature soils in the upper catchment in MIS 5. Overall, we assume that erosivity in the mountainous regions was reduced while coastal erosion was increased during MIS 6. Hou et al. (2020b) proposed that very strong trade winds caused prolonged SST warming in the western tropical South Atlantic during late MIS 6. The presence of strong trade winds and high SSTs, which increase coastal precipitation, could reinforce the enhanced mature lowland soil erosion indicated by the low parent rock derived to soil-built phase ratio, the illite to kaolinite ratio and the illite mineral parameters (**Figure 4**).

As the overall sediment discharge remained insolation dependent, it is likely that moisture availability was also increased in the Doce watershed during the high insolation phases of MIS 6. The lack of immature soil derived mineral phases during periods of high moisture availability indicates a difference in the distribution and short-term precipitation intensity between MIS 5 and MIS 6. Precipitation anomalies related to the modern SASM are more intense in the upper catchment of the Doce River (**Figure 1**). The sediment load discharged during December and January is roughly twice as much as the combined load during the rest of the year (Oliveira & Quaresma, 2017). Thus, monsoon-related heavy precipitation events in the upper catchment contribute largely to today's sediment discharge. A similar discharge pattern can explain the mineral assemblage of the high insolation phases in MIS 5 but not in MIS 6. The insolation-dependent increase in sediment influx to the ocean during MIS 6 comprised mostly soil-built phases. This points towards low precipitation intensity and erosivity in the upper river course in favor of more evenly distributed precipitation over the kaolinite-rich, mature soil layers of the Doce Basin and increased lowland erosion. We propose that during MIS 6 precipitation in the mountainous areas was reduced and fewer heavy precipitation events occurred, compared to MIS 5. Therefore, it is likely that the summer monsoon system along the SACZ was poorly developed throughout MIS 6, even during periods of high insolation.

High Northern Latitude Temperatures and Local Precipitation

The difference in discharge composition between glacial (MIS 6) and interglacial (MIS 5) seen in our data agrees with previous studies indicating that the mainly insolation driven precipitation patterns over SE Brazil are affected by high northern latitude temperature changes and global pCO$_2$ (Cruz et al., 2005, 2009; Hou et al., 2020a). We assume that during MIS 6, lowland winter

precipitation in the Doce Basin was higher and the region experienced less intense but more frequent precipitation all year round, eroding more mature lowland soils and less immature mountainous soils. Moreover, our data show reduced summer monsoon precipitation during MIS 6. A driver of reduced summer precipitation in the Doce Basin could be a weakened SACZ caused by reduced AMOC during MIS 6, leading to higher temperatures at the SW Atlantic and shifting the sea-land interaction and thus the strength of the convection belts, as previously described for eastern Brazil during reduced AMOC phases of the Holocene (Bahr et al., 2021).

From our data, we can infer that the predominant rainfall regime in the Doce Basin shifted from well-developed lowland and coastal precipitation in MIS 6 to insolation-dependent heavy summer monsoon precipitation in the mountainous regions during MIS 5. Similarly, precipitation models propose that by 2080 global warming will have induced a slight increase in summer precipitation in the Doce watershed while winter precipitation will be decreased (FEAM, 2011; IPCC, 2021). Flooding associated with particularly heavy monsoonal summer precipitation and accurate flood forecasts are already a problem in the Doce watershed (Tomasella et al., 2019); an increase in heavy precipitation events would exacerbate this issue. Our data further indicate that riverine discharge was mostly insolation-dependent during interglacial periods. However, the observed shift in the precipitation pattern from glacial to interglacial conditions suggest that the likelihood of heavy precipitation events in the mountainous areas could increase and SE trade wind induced precipitation in the coastal areas could decrease with global warming. The trends seen in our paleoenvironmental data are in line with climate model precipitation predictions, underlining the need to prepare the region for increasing monsoonal heavy precipitation events and lowland droughts. We suggest further investigations on the spatial distribution of paleoprecipitation in the region, to test this hypothesis and to expand upon the understanding of climate-related precipitation changes in the Doce watershed area.

CONCLUSION

The availability in terrestrial sediment input from the Doce River to the marine sediment core M125-55-7 shows that insolation changes primarily paced fluvial discharge during the interval from 150 to 70 ka before present. Changes in the mineralogical composition of the discharge indicate that a strong summer monsoon system developed during the high austral summer insolation phases of the interglacial MIS 5, wherein heavy precipitation events increased erosion in the mountainous regions. During the low summer insolation phases of MIS 5, the monsoonal system was weakened, and lowland erosion became the main supplier of detrital fluvial discharge. During the glacial interval MIS 6, lowland and coastal erosion dominated the discharged sediment. A strong monsoonal precipitation pattern, increasing erosion in mountainous regions, was not developed. We propose that during MIS 5, the austral summer monsoon system strengthened and weakened in phase with insolation along a stationary SACZ. In contrast, the summer monsoon system throughout (late) MIS 6 was poorly developed,

even in times of high insolation. Therefore, the impact of lowland precipitation on the riverine discharge was dominant throughout MIS 6. In this study, we interpret relative changes in riverine discharge. For a quantitative comparison with present and future climate scenarios, further research is needed. From the qualitative assessment of our paleoenvironmental data, we can infer that global warming may lead to more erosive SASM-related heavy precipitation events in summer and reduced mean annual precipitation in the lowland. This inference corresponds to recent climate models (IPCC, 2021), indicating that with ongoing anthropogenic global warming, the region of the Doce watershed will become more vulnerable to both flooding and droughts.

DATA AVAILABILITY STATEMENT

The original contributions presented in the study are included in the article/**Supplementary Material**, further inquiries can be directed to the corresponding author.

AUTHOR CONTRIBUTIONS

FUNDING

ACKNOWLEDGMENTS

SUPPLEMENTARY MATERIAL

The Supplementary Material for this article can be found online at: https://www.frontiersin.org/articles/10.3389/feart.2022.864381/full#supplementary-material

Data Sheet 1 | bulk sediment texture free XRD data

Data Sheet 2 | clay fraction texture free XRD data

Data Sheet 3 | clay fraction textured XRD data

Data Sheet 4 | mineralogical parameters of illite

REFERENCES

Abreu Jr., C. H., Jr., Muraoka, T., and Lavorante, A. F. (2003). Relationship between Acidity and Chemical Properties of Brazilian Soils. *Sci. Agric. (Piracicaba, Braz.)* 60, 337–343. doi:10.1590/S0103-90162003000200019

Almeida, F. F. M. d., Brito Neves, B. B. d., and Dal Ré Carneiro, C. (2000). The Origin and Evolution of the South American Platform. *Earth-Science Rev.* 50, 77–111. doi:10.1016/S0012-8252(99)00072-0

Alvares, C. A., Stape, J. L., Sentelhas, P. C., de Moraes Gonçalves, J. L., Sparovek, G., Arp, G., et al. (2013). Köppen's Climate Classification Map for BrazilPhotosynthesis-Induced Biofilm Calcification and Calcium Concentrations in Phanerozoic Oceans. *metzScience* 22292, 7111701–7281704. doi:10.1126/science.105720410.1127/0941-2948/2013/0507

Bahr, A., Doubrawa, M., Titschack, J., Austermann, G., Nürnberg, D., Albuquerque, A. L., et al. (2020). Monsoonal Forcing Controlled Cold Water Coral Growth off South-Eastern Brazil during the Past 160 Kyrs. *Paleobiogeoscience Clim. Connect.* doi:10.5194/bg-2020-206

Bahr, A., Kaboth-Bahr, S., Jaeschke, A., Chiessi, C., Cruz, F., Carvalho, L., et al. (2021). Late Holocene Precipitation Fluctuations in South America Triggered by Variability of the North Atlantic Overturning Circulation. *Paleoceanogr. Paleoclimatol* 36, e2021PA004223. doi:10.1029/2021PA004223

Bahr, A., Spadano Albuquerque, A. L., Ardenghi, N., Batenburg, S. J., Bayer, M., Catunda, M. C., et al. (2016). South American Hydrological Balance and Paleoceanography during the Late Pleistocene and Holocene (SAMBA)-Cruise No. M125, *March 21-April 15, 2016 – Rio J. (Brazil)-Fortaleza Braz.* (Bremen (Germany): METEOR-Berichte M125), 54, 34. doi:10.2312/cr_m125

Bastos, A. C., Amado-Filho, G. M., Moura, R. L., Sampaio, F. M., Bassi, D., and Braga, J. C. (2016). Origin and Sedimentary Evolution of Sinkholes (Buracas) in the Abrolhos Continental Shelf, Brazil. *Palaeogeogr. Palaeoclimatol. Palaeoecol.* 462, 101–111. doi:10.1016/j.palaeo.2016.09.009

Biscaye, P. E. (1965). Mineralogy and Sedimentation of Recent Deep-Sea Clay in the Atlantic Ocean and Adjacent Seas and Oceans. *Geol. Soc. Am. Bull.* 76, 803–832. doi:10.1130/0016-7606(1965)76[803

Bliss, N. (2013). *LBA-ECO LC-08 Soil, Vegetation, and Land Cover Maps for Brazil and South America. Data Set.* Oak Ridge, Tennessee, U.S.A. Available on-line (from Oak Ridge National Laboratory Distributed Active Archive Center Available at: http://daac.ornl.gov.

Carvalho, L. M. V. (2020). Assessing Precipitation Trends in the Americas with Historical Data: A Review. *WIREs Clim. Change* 11, e627. doi:10.1002/wcc.627

Costa, K. B., Cabarcos, E., Santarosa, A. C. A., Battaglin, B. B. F., and Toledo, F. A. L. (2016). A Multiproxy Approach to the Climate and Marine Productivity Variations along MIS 5 in SE Brazil: A Comparison between Major Components of Calcareous Nannofossil Assemblages and Geochemical Records. *Palaeogeogr. Palaeoclimatol. Palaeoecol.* 449, 275–288. doi:10.1016/j.palaeo.2016.02.032

CPRM – Serviço Geológico do Brasil (2004). *Geological Map of Brazil 1:1.000.000 Scale: Geographic Information System-GIS.* Brasília: CPRM.

Cruz, F. W., Burns, S. J., Karmann, I., Sharp, W. D., Vuille, M., Cardoso, A. O., et al. (2005). Insolation-driven Changes in Atmospheric Circulation over the Past 116,000 Years in Subtropical Brazil. *Nature* 434, 63–66. doi:10.1038/nature03365

Cruz, F. W., Vuille, M., Burns, S. J., Wang, X., Cheng, H., Werner, M., et al. (2009). Orbitally Driven East-West Antiphasing of South American Precipitation. *Nat. Geosci.* 2, 210–214. doi:10.1038/ngeo444

Cunha, A. d. M., Fontes, M. P. F., and Lani, J. L. (2019). Mineralogical and Chemical Attributes of Soils from the Brazilian Atlantic Forest Domain. *Sci. Agric. (Piracicaba, Braz.)* 76, 82–92. doi:10.1590/1678-992x-2017-0109

Embrapa-SNLCS (1981). *Mapa des Solos do Brasil, 1:5.000.000.* Rio de Janeiro (Brazil): Empresa Brasileira de Pesquisa Agropecuária - Serviço Nacional de Levantamento e Conservação de solos.

Esquevin, J. (1969). Influence de la composition chimique des illites sur leur cristallinité. *Bull. Cent. Researches Pau-SNPA* 3, 147–153.

FAO-UNESCO (1971). *Soil Map of the World, 1:5.000.000.* Paris (France): South America.

FEAM (2011). *Avaliação de impactos de mudanças climáticas sobre a economia mineira: relatório resumo.*

Flantua, S. G. A., Hooghiemstra, H., Vuille, M., Behling, H., Carson, J. F., Gosling, W. D., et al. (2016). Climate Variability and Human Impact in South America during the Last 2000 years: Synthesis and Perspectives from Pollen Records. *Clim. Past.* 12, 483–523. doi:10.5194/cp-12-483-2016

Gerhardt, S., and Henrich, R. (2001). Shell Preservation of Limacina Inflata (Pteropoda) in Surface Sediments from the Central and South Atlantic Ocean: A New Proxy to Determine the Aragonite Saturation State of Water Masses. *Deep Sea Res. Part I Oceanogr. Res. Pap.* 48, 2051–2071. doi:10.1016/S0967-0637(01)00005-X

Grathoff, G. H., and Moore, D. M. (1996). Illite Polytype Quantification Using WILDFIRE Calculated X-Ray Diffraction Patterns. *Clays Clay Minerals* 44, 835–842. doi:10.1346/CCMN.1996.0440615

GRDC (2020). *Major River Basins of the World/Global Runoff Data Centre, GRDC. 2nd, Rev. Ext.* Koblenz, Germany: Federal Institute of Hydrology BfG.

Henrich, R., Baumann, K.-H., Gerhardt, S., Gröger, M., and Volbers, A. (2003). Carbonate Preservation in Deep and Intermediate Water Masses in the South Atlantic: Evaluation and Geological Record (A Review), 645, 670. doi:10.1007/978-3-642-18917-3_28

Hou, A., Bahr, A., Raddatz, J., Voigt, S., Greule, M., Albuquerque, A. L., et al. (2020a). Insolation and Greenhouse Gas Forcing of the South American Monsoon System across Three Glacial-Interglacial Cycles. *Geophys. Res. Lett.* 47, e2020GL087948. doi:10.1029/2020GL087948

Hou, A., Bahr, A., Schmidt, S., Strebl, C., Albuquerque, A. L., Chiessi, C. M., et al. (2020b). Forcing of Western Tropical South Atlantic Sea Surface Temperature across Three Glacial-Interglacial Cycles. *Glob. Planet. Change* 188, 103150. doi:10.1016/j.gloplacha.2020.103150

IPCC (2021). *Climate Change 2021: The Physical Science Basis. Contribution of Working Group I to the Sixth Assessment Report of the Intergovernmental Panel on Climate Change.*

Jaeschke, A., Rühlemann, C., Arz, H., Heil, G., and Lohmann, G. (2007). Coupling of Millennial-Scale Changes in Sea Surface Temperature and Precipitation off Northeastern Brazil with High-Latitude Climate Shifts during the Last Glacial Period. *Paleoceanography* 22, a–n. doi:10.1029/2006PA001391

Jahnke, R. A., Craven, D. B., and Gaillard, J.-F. (1994). The Influence of Organic Matter Diagenesis on CaCO3 Dissolution at the Deep-Sea Floor. *Geochimica Cosmochimica Acta* 58, 2799–2809. doi:10.1016/0016-7037(94)90115-5

Jones, C., and Carvalho, L. M. V. (2002). Active and Break Phases in the South American Monsoon System. *J. Clim.* 15, 905–914. doi:10.1175/1520-0442(2002)015<0905:AABPIT>2.0

Jones, G. A. (1984). Advective Transport of Clay Minerals in the Region of the Rio Grande Rise. *Mar. Geol.* 58, 187–212. doi:10.1016/0025-3227(84)90123-3

Kanner, L. C., Burns, S. J., Cheng, H., and Edwards, R. L. (2012). High-Latitude Forcing of the South American Summer Monsoon during the Last Glacial. *Science* 335, 570–573. doi:10.1126/science.1213397

Knutti, R., and Sedláček, J. (2013). Robustness and Uncertainties in the New CMIP5 Climate Model Projections. *Nat. Clim. Change* 3, 369–373. doi:10.1038/nclimate1716

Kodama, Y. (1992). Large-Scale Common Features of Subtropical Precipitation Zones (The Baiu Frontal Zone, the SPCZ, and the SACZ) Part I: Characteristics of Subtropical Frontal Zones. *J. Meteorological Soc. Jpn.* 70, 813–836. doi:10.2151/jmsj1965.70.4_813

Kranz, S. A., Gladrow, D. W., Nehrke, G., Langer, G., and Rosta, B. (2010). Calcium Carbonate Precipitation Induced by the Growth of the Marine Cyanobacteria Trichodesmium. *Limnol. Oceanogr.* 55, 2563–2569. doi:10.4319/lo.2010.55.6.2563

Laskar, J., Robutel, P., Joutel, F., Gastineau, M., Correia, A. C. M., and Levrard, B. (2004). A Long-Term Numerical Solution for the Insolation Quantities of the Earth. *A&A* 428, 261–285. doi:10.1051/0004-6361:20041335

Lima, J. E. F. W., Lopes, W. T. A., Carvalho, N. O., Vieira, M. R., and Silva, E. M. (2005). "Suspended Sediment Fluxes in the Large River Basins of Brazil," in *Sediment Budgets 1, Proceedings of the Foz Do Iguaçu Symposium, IAHS Scientific Assembly* (Foz do Iguaçu (Brazil): IAHS Publ.), 355–363.

Lisiecki, L. E., and Raymo, M. E. (2005). A Pliocene-Pleistocene Stack of 57 Globally Distributed Benthic δ18O Records. *Paleoceanography* 20, a–n. doi:10.1029/2004PA001071

Maiada, R. M. d. C. C., Reisdos, A. T. d., Alvesda, E. d. C. C., Silva, C. G., Guerra, J. V., Gorini, C., et al. (2010). Architecture and stratigraphic framework of shelf sedimentary systems off Rio de Janeiro state, Northern Santos Basin-Brazil. *Braz. J. Oceanogr.* 58, 15–29. doi:10.1590/S1679-87592010000500003

May, P., Alonso, L., Barbosa, F., Brito, M. C., Laureano, F., Maroun, C., et al. (2020). Mainstreaming Climate Change in the Rio Doce Watershed Restoration. Available at: https://portals.iucn.org/library/node/49066 (Accessed November 22, 2021). doi:10.2305/iucn.ch.2020.06.en

Melfi, A. J., Cerri, C. C., Kronberg, B. I., Fyfe, W. S., and McKinnon, B. (1983). Granitic Weathering: a Brazilian Study. *J. Soil Sci.* 34, 841–851. doi:10.1111/j.1365-2389.1983.tb01076.x

Melo, V. F., Singh, B., Schaefer, C. E. G. R., Novais, R. F., and Fontes, M. P. F. (2001). Chemical and Mineralogical Properties of Kaolinite-Rich Brazilian Soils. *Soil Sci. Soc. Am. J.* 65, 1324–1333. doi:10.2136/sssaj2001.6541324x

Meunier, A., and Velde, B. (2004). "The Geology of Illite," in *Illite: Origins, Evolution and Metamorphism*. Editors A. Meunier and B. Velde (Berlin, Heidelberg: Springer), 63–143. doi:10.1007/978-3-662-07850-1_3

Mohr, E. C. J., Van Baren, F. A., and Van Schuylenborgh, J. (1972). *Tropical Soils – A Comprehensive Study of Their Genesis*. 3rd ed. The Hague (Netherlands): Mouton - Ichtiar Baru - Van Hoeve.

Oliveira, E. N. d., Knoppers, B. A., Lorenzzetti, J. A., Medeiros, P. R. P., Carneiro, M. E., and Souza, W. F. L. d. (2012). A Satellite View of Riverine Turbidity Plumes on the NE-E Brazilian Coastal Zone. *Braz. J. Oceanogr.* 60, 283–298. doi:10.1590/S1679-87592012000300002

Oliveira, K. S. S., and Quaresma, V. d. S. (2017). Temporal Variability in the Suspended Sediment Load and Streamflow of the Doce River. *J. S. Am. Earth Sci.* 78, 101–115. doi:10.1016/j.jsames.2017.06.009

Petit, J. R., Jouzel, J., Raynaud, D., Barkov, N. I., Barnola, J.-M., Basile, I., et al. (1999). Climate and Atmospheric History of the Past 420,000 Years from the Vostok Ice Core, Antarctica. *Nature* 399, 429–436. doi:10.1038/20859

Petró, S. M., Pivel, M. A. G., and Coimbra, J. C. (2021). Evidence of Supra-lysoclinal Dissolution of Pelagic Calcium Carbonate in the Late Quaternary in the Western South Atlantic. *Mar. Micropaleontol.* 166, 102013. doi:10.1016/j.marmicro.2021.102013

Petschick, R., Kuhn, G., and Gingele, F. (1996). Clay Mineral Distribution in Surface Sediments of the South Atlantic: Sources, Transport, and Relation to Oceanography. *Mar. Geol.* 130, 203–229. doi:10.1016/0025-3227(95)00148-4

Petschick, R. (2010). *MacDiff 4.2.6 Manual*. Available at: http://www.uni-frankfurt.de/69528130/Petschick___MacOS_Software.

Raddatz, J., Titschack, J., Frank, N., Freiwald, A., Conforti, A., Osborne, A., et al. (2020). Solenosmilia Variabilis-Bearing Cold-Water Coral Mounds off Brazil. *Coral Reefs* 39, 69–83. doi:10.1007/s00338-019-01882-w

Riding, R. (2000). Microbial Carbonates: the Geological Record of Calcified Bacterial-Algal Mats and Biofilms. *Sedimentology* 47, 179–214. doi:10.1046/j.1365-3091.2000.00003.x

Rind, D. (1998). Latitudinal Temperature Gradients and Climate Change. *J. Geophys. Res.* 103, 5943–5971. doi:10.1029/97JD03649

P. A. Sanchez (Editor) (2019). "Mineralogy," *Properties and Management of Soils in the Tropics* (Cambridge: Cambridge University Press), 196–209. doi:10.1017/9781316809785.010

Santos, E. O. de J., Gontijo, I., and Silva, M. B. da. (2014). Spatial Variability of Soil Acidity Attributes and Liming Requirement for Conilon Coffee. *Coffee Sci.* 9, 275–283. Available at: http://www.sbicafe.ufv.br/handle/123456789/8052. (Accessed April 22, 2022).

Schlitzer, R. (2021). Ocean Data View (ODV). Available at: https://odv.awi.de/ (Accessed April 22, 2022).

Schobbenhaus, C., Campos, D. de A., Derze, G. R., and Asmus, H. E. (1981). *Geologic Map of Brazil and Adjoining Ocean Floor Including Mineral Deposits, Scale 1: 1500 000*. Brasilia: Departamento Nacional da Producao Mineral.

Seo, K.-H., Frierson, D. M. W., and Son, J.-H. (2014). A Mechanism for Future Changes in Hadley Circulation Strength in CMIP5 Climate Change

Simulations. *Geophys. Res. Lett.* 41, 5251–5258. doi:10.1002/2014GL060868

Souza, W. F. L., and Knoppers, B. (2011). Fluxos de água e sedimentos a costa leste Do Brasil: relações entre a tipologia e as pressões antrópicas. *Geochim. Bras.* 17, 57–74.

Spratt, R. M., and Lisiecki, L. E. (2016). A Late Pleistocene Sea Level Stack. *Clim. Past.* 12, 1079–1092. doi:10.5194/cp-12-1079-2016

Stríkis, N. M., Chiessi, C. M., Cruz, F. W., Vuille, M., Cheng, H., Souza Barreto, E. A., et al. (2015). Timing and Structure of Mega-SACZ Events during Heinrich Stadial 1. *Geophys. Res. Lett.* 42, 5477–5484A. doi:10.1002/2015GL064048

Stríkis, N. M., Cruz, F. W., Barreto, E. A. S., Naughton, F., Vuille, M., Cheng, H., et al. (2018). South American Monsoon Response to Iceberg Discharge in the North Atlantic. *Proc. Natl. Acad. Sci. U.S.A.* 115, 3788–3793. doi:10.1073/pnas.1717784115

Suárez-Ibarra, J. Y., Frozza, C. F., Palhano, P. L., Petró, S. M., Weinkauf, M. F. G., and Pivel, M. A. G. (2022). Calcium Carbonate Dissolution Triggered by High Productivity during the Last Glacial-Interglacial Interval in the Deep Western South Atlantic. *Front. Earth Sci.* 10. doi:10.3389/feart.2022.830984

Thiry, M. (2000). Palaeoclimatic Interpretation of Clay Minerals in Marine Deposits: an Outlook from the Continental Origin. *Earth-Science Rev.* 49, 201–221. doi:10.1016/S0012-8252(99)00054-9

Tierney, J. E., Poulsen, C. J., Montañez, I. P., Bhattacharya, T., Feng, R., Ford, H. L., et al. (2020). Past Climates Inform Our Future. *Science* 370. doi:10.1126/science.aay3701

Tintelnot, M. (1995). *Transport and Deposition of Fine-Grained Sediments on the Brazilian Continental Shelf as Revealed by Clay Mineral Distribution*.

Tomasella, J., Sene Gonçalves, A., Schneider Falck, A., Oliveira Caram, R., Rodrigues Diniz, F. l., Rodriguez, D. a., et al. (2019). Probabilistic Flood Forecasting in the Doce Basin in Brazil: Effects of the Basin Scale and Orientation and the Spatial Distribution of Rainfall. *J. Flood Risk Manag.* 12, e12452. doi:10.1111/jfr3.12452

B. Velde (Editor) (1995). *Origin and Mineralogy of Clays: Clays and the Environment* (Berlin, Heidelberg: Springer). doi:10.1007/978-3-662-12648-6

Velde, B., and Meunier, A. (2008). "Fundamentals of Clay Mineral Crystal Structure and Physicochemical Properties," in *The Origin of Clay Minerals in Soils and Weathered Rocks*. Editors B. Velde and A. Meunier (Berlin, Heidelberg: Springer), 3–73. doi:10.1007/978-3-540-75634-7_1

Vuille, M., and Garreaud, R. D. (2011). "Ocean-atmosphere Interactions on Interannual to Decadal Timescales," in *Handbook of Environmental Change* (Los Angeles, New Delhi, Singapore: Sage Publications London), 471–496.

Warratz, G., Henrich, R., Voigt, I., Chiessi, C. M., Kuhn, G., and Lantzsch, H. (2017). Deglacial Changes in the Strength of Deep Southern Component Water and Sediment Supply at the Argentine Continental Margin. *Paleoceanography* 32, 796–812. doi:10.1002/2016PA003079

WRB, IUSS Working Group (2015). World Reference Base for Soil Resources 2014, Update 2015 International Soil Classification System for Naming Soils and Creating Legends for Soil Maps. *World Soil Resour. Rep. No.* 106, 192.